Probing maltodextrins surface properties by atomic force microscopy: Interplay of glass transition and reconstitution properties

Regis Badin, Jennifer Burgain, Stephane Desobry, Bhesh Bhandari, Sangeeta Prakash, Claire Gaiani

PROBING MALTODEXTRINS SURFACE PROPERTIES BY ATOMIC FORCE MICROSCOPY: INTERPLAY OF GLASS TRANSITION AND RECONSTITUTION PROPERTIES

Regis Badin[a], Jennifer Burgain[a], Stephane Desobry[a], Bhesh Bhandari[b], Sangeeta Prakash[b], Claire Gaiani[a,c]

[a] Université de Lorraine, LIBio, Nancy, F-54000, France

[b] School of Agriculture and Food Sciences, The University of Queensland, Brisbane, Queensland 4072, Australia

[c] Institut Universitaire de France (IUF)

Corresponding author: claire.gaiani@univ-lorraine.fr

Highlights:

- Glass transition significantly impacted maltodextrin reconstitution properties
- Surface topographies revealed surface smoothing above glass transition
- Surface nanoscale hollow formation was observed at the rubbery state
- Young modulus decreased significantly at the rubbery state

Abstract

Reconstitution kinetics of three maltodextrins powders with different dextrose-equivalent (DE) values (low, intermediate, high DE) were evaluated under the glassy and rubbery states. Reconstitution times were found mostly shear rate of agitation in water and DE dependent in

the glassy state, with shorter reconstitution times for high shear rates and DE. For powders under the rubbery state, reconstitution times were less shear rate dependent, especially for high DE values. To have a better understanding of powder surface features that can impact reconstitution properties, single particles surface topographies and nanomechanical properties were probed by Atomic Force Microscopy (AFM). It was shown that surface roughness was higher for high DE maltodextrins under the glassy state, whereas a surface smoothing and slight hollows formation was observed for all powders under the rubbery state. Also, a significant reduction and uniformity of Young modulus at the particle surface were observed under the rubbery state. Finally, surface modification at microscale (smoothing and softening) was linked to powder behavior evolution at macroscale (relative shear rate independence during reconstitution) when the powder crosses the glass transition.

Keywords: Maltodextrin, Reconstitution, Glass transition, Powder, Surface topography, Nanoindentation.

1. INTRODUCTION

Powdered ingredients are involved in many manufacturing products and regularly used in the food industry, primarily for their ease of use, handling, transport and extended storage properties (Bhandari, 2013; Gaiani, Burgain, & Scher, 2013). Powders originate from the conversion of a liquid into a solid by various drying methods (such as spray-drying, freeze-drying, crystallization) or from size reduction processes (such as grinding, crushing, milling) (Bhandari, 2013; Islam & Langrish, 2013; Ratti, 2013; Woo & Bhandari, 2013). Because of these various origins and natures, powders physicochemical properties can be highly variable, thus influencing their technofunctional properties.

Reconstitution ability of dehydrated products in aqueous media is one of the most relevant functionalities to describe when one talk about food powders for industrial applications (Crowley, Kelly, Schuck, Jeantet, & O'Mahony, 2016; Gaiani et al., 2007a; Selomulya & Fang, 2013). For industrial applications, but also at the consumer level, quick and complete reconstitution properties are generally prerequisites (Forny, Marabi, & Palzer, 2011; Fournaise, Petit, & Gaiani, 2021). For example, coating or agglomeration processes are oftently used by industrials to improve powder reconstitution (Barringer, 2013; Cuq & Mandato, 2013; Gaiani, Schuck, Scher, Desobry, & Banon, 2007b). Powder reconstitution is a complex process that can be generally divided into four main steps including wetting, sinking, dispersion and solubilization, which may sometimes occur concurrently (Crowley et al., 2016; Fitzpatrick et al., 2016; Fitzpatrick, Ji, & Mao, 2021; Forny, et al., 2011; Gaiani et al., 2007a; Mitchell et al., 2014). Reconstitution conditions (e.g., shear rate, temperature, viscosity), particle size, shape, and porosity, highly influence reconstitution kinetics (Selomulya & Fang, 2013; Crowley et al., 2016).

The glass transition is one of the most critical parameters to consider during powders processing and storage. At a critical temperature, molecular mobility increases when an

amorphous solid undergoes from a glassy to a rubbery state (Fitzpatrick et al., 2007; Roos & Drusch, 2016; Roudaut, Simatos, Champion, Contreras-Lopez, Le Meste, 2004; Yoshioka & Aso, 2007). This event is also highly dependent on relative humidity, as water plays the role of a plasticizer. An increase of water content in the food powder is highly responsible for a decrease in the glass transition temperature (Tg) (Roos, 2002; 2006). This phenomenon consequently impacts powder properties. Particles become stickier because of increased surface energy, enhancing interactions with materials that are in contact with powder surface. Powders are also susceptible to forming strong cakes under the rubbery state (Fitzpatrick et al., 2007) and time-dependent crystallization phenomenon can occur (Wang & Truong, 2017). Glass transition is also accompanied by a significant decrease of the Young modulus at the particle surface (Palzer, 2007). Thus, particle surface elastic behavior drastically changes when the powder surface reaches the glass transition temperature.

Knowing that the powder surface is the first layer in contact with water during powder reconstitution, this later layer is expected to play a major role in this process. Powder surface is therefore highly dependent on environmental conditions (i.e., temperature and relative humidity). In the past decade, numerous powder surface analysis techniques have been used to further understand the role of the particle surface on the impairments of powder functionalities. For example, microscopy techniques such as Scanning Electron Microscopy, Confocal Laser Scanning Microscopy or even chemical composition techniques such as X-ray Photoelectron Spectroscopy are already widely used (Burgain et al., 2017; Murrieta-Pazos et al., 2012). Atomic Force Microscopy (AFM) is currently a rising star in the food powder surface analysis field, mainly due to its high-resolution capacity. AFM is such an unusual microscopy technique based on the use of a probe (mounted on a cantilever), which can reconstruct the surface topography by sweeping the sample surface. This system gives AFM its characteristic nanoscale sensitivity as the probe can record nanoscale height variation

thanks to a laser reflected towards the probe and detected by a photodiode (Burgain et al., 2017; Dufrene, 2002). AFM exhibits many advantages, such as nanoscale sensitive resolution capacity or the ability to analyze samples without pretreatment or vacuum conditions. Additionally, AFM is also a versatile tool compared to other surface analysis techniques, as it allows to estimate surface roughness. For example, Burgain et al. (2016a) were able to better understand surface modifications during high-temperature storage of whey protein isolate powders. They studied surface roughness and highlighted the formation of hollow structures related to improper storage conditions. Murrieta-Pazos et al. (2011) also used AFM to investigate the particle structure and roughness of skim and whole milk powders evolution during water adsorption. In addition to the topographical information, one of the other major assets of this technique is its ability to study nanomechanical properties due to nanoindentation experiments (Butt, Cappella, & Kappl, 2005; Gaboriaud & Dufrene 2007). This technique allows the detection of very localized variations of surface elasticity, as data are then useful for building highly resolutive elasticity maps. Despite all these advantages, powder nanoindentation experiments by AFM are mainly developed in the pharmaceutical field to relate particle hardness to powder tableting and compaction (Wu, Li, & Mansour, 2010), to characterize mechanical properties of excipients particles (Liao & Wiedmann, 2003; Masterson & Cao, 2008; Perkins et al., 2007; Ramos & Bahr, 2007) or to study particle-particle interactions in inhaled powders formulations (Arora et al., 2016; Berard et al., 2002; Traini, Young, Rogueda, & Price, 2006; Weiss, McLoughlin, & Cathcart, 2015; Young, Tobyn, Price, Buttrum, & Dey, 2006). On the contrary, regarding the application in the food powder field, nanoindentation experiments are scarcely used (Burgain, Scher, Petit, Francius, & Gaiani, 2016b; Haider et al., 2013; Prime, Stapley, Rielly, Jones, & Leaper, 2011a; Prime et al., 2011b). Knowing that AFM brings at the same time topographical and mechanical

112 information of powder surface at the particle scale, this technique could be relevant to obtain
113 a deeper understanding of powders functionalities, such as reconstitution.

114 Carbohydrate-based powders, especially maltodextrins, can be found in many products and
115 are widely used in the food industry as thickener agents, for flavour enhancement, film-
116 forming properties, encapsulating agents or even as excipients in pharmaceutical products
117 (Castro, Durrieu, Raynaud, & Rouilly, 2016; Descamps, Palzer, Roos, & Fitzpatrick, 2013;
118 Li, Pan, Ma, Miao, & Ji, 2020). Maltodextrins are polymer chains produced by the hydrolysis
119 of starch. They are generally classified by their polymer chain length, estimated by the
120 Dextrose Equivalent (DE) value (Avaltroni, Bouquerand, & Normand, 2004; Chronakis,
121 1998). The different DE values are related to the hydrolysis degree and show very distinct
122 functional properties. Low DE maltodextrins exhibit high viscosity and high Tg, whereas high
123 DE maltodextrins exhibit low viscosity and low Tg (Castro et al., 2016; Rong, Sillick, &
124 Gregson, 2009; Siemons, Politiek, Boom, van der Sman, & Schutyser, 2020). This makes the
125 choice of the DE of the maltodextrin matrix crucial. For example, mixtures with added
126 maltodextrins are commonly used on food powder to master the glass transition temperature
127 (Fongin, Kawai, Harnkarnsujarit, & Hagura, 2017; Frascareli, Silva, Tonon, & Hubinger,
128 2012; Shrestha, Ua-arak, Adhikari, Howes, & Bhandari, 2007). Moreover, maltodextrins are
129 highly susceptible to caking phenomena, and their reconstitution properties are highly
130 dependent on the DE value. Indeed, high DE maltodextrins reconstitute faster (Dupas, Girard,
131 & Forny, 2017; Descamps et al., 2013).

132 Bringing new information about maltodextrins surface properties and the interplay between
133 physical state and reconstitution properties is relevant to optimize powder uses in the food
134 industry. The present study aims to provide a deeper understanding of maltodextrins
135 reconstitution properties, depending on their physical state and molecular chain length (or
136 DE), while bringing new insights about particle surface properties using AFM.

2. MATERIAL AND METHODS

2.1. Material

Maltodextrin powders with three different DE values were employed in the present study. Higher DE values correspond to more enzymatically hydrolyzed products than those with lower DE values. Spray-dried maize maltodextrins with DE 4-7 (i.e., low DE) and 16.5-19 (i.e., high DE) were purchased from Sigma-Aldrich (Saint-Louis, Missouri, USA) and those with DE 12 (i.e., intermediate DE) were purchased from Roquette Frères (Lestrem, France). Maltodextrins were chosen to cover a range of DE between 4 and 19. DE values higher than 20 are considered to be dextrins or glucose syrups (Chronakis, 1998) which usually are in a liquid state.

2.2. Powder physical properties

2.2.1. Glass transition temperature (T_g)

Differential Scanning Calorimetry (DSC) was used to determine the Tg. DSC was calibrated using Indium metal as a standard. For the calibration, 5 repetitions were made, each with 3 sequent heating segments and with a heating rate of 20 °C/min. A first heating ramp from 20 to 210 °C was performed, followed by a cooling to 50 °C. Then, a second heating ramp from 50 to 210 °C and another cooling to 50 °C was also done. A third and final heating ramp to 210 °C was also performed. Finally, to ensure good DSC calibration, onset melting point was determined on the second and third heating curves. This later should be measured at 156.6 °C within a range of 0.2 °C.

Powders samples were first equilibrated at different water activities (a_w) thanks to a climatic chamber (Climacell, MMM Medcenter, Fisher Bioblock Scientific, Illkirch, France), which allowed to control relative humidity (RH) and temperature. For this purpose, powders were deposited under a thin layer on petri dishes to allow RH and temperature equilibrium.

When the equilibrium relative humidity (ERH) is reached, a_w is equal to the ERH divided by 100 (i.e. $a_w = ERH/100$). Thus, a_w can be adjusting by controlling the relative humidity (Kong & Singh, 2016). In order to reach very low a_w, phosphorus pentoxide (P_2O_5) was employed for equilibrium which is known to be a desiccant salt (0% RH).

Before DSC experiments (DSC2500 discovery series from TA Instruments, Hüllhorst, Germany), a_w was measured for each sample thanks to a HygroPalm23-a_w portable device (Rotronic, France) at room temperature (22 ± 2 °C).

Equilibrated powders (10 – 15 mg) were hermetically sealed in aluminium Tzero pans (TA Instruments, Hüllhorst, Germany). An empty pan was used as a reference and nitrogen as a carrier gas. Samples were first equilibrated for 1 min at - 60 °C. This step was followed by a first heating ramp up to 180 °C (10 °C/min) in order to erase the thermal history of the sample. Pans were then equilibrated for 1 min at 180 °C and cooled to the initial temperature of - 60 °C (10 °C/min). A second heating ramp was finally performed up to 180 °C (10 °C/min).

T_g was determined thanks to the heat flow change on the second heating ramp with the TRIOS analysis software (TA Instruments, Hüllhorst, Germany). The half slope height method was used to calculate the midpoint T_g. The onset and endset point of the glass transition events were also determined. All measurements were performed in triplicate and T_g values were averaged.

2.2.2. Particle size distribution

The particle size distribution was analyzed using a Mastersizer MS3000 (Malvern Instruments, UK) with Aero S air unit which allows powder dispersion. In order to obtain a good laser obscuration, analytical conditions were defined with the following parameters: air pressure at 2 bars, hopper length of 2 mm, powder feed rate between 20 - 30%. Finally,

185 classical descriptors were used to estimate particle size distributions (D_{10}, D_{50}, D_{90}). These
186 parameters represent the diameters for which 10%, 50% or 90% have lower sizes. The Span
187 was also used to estimate the width of the particle size distribution and is calculated thanks to
188 **Equation 1**. Experiments were performed in triplicate.

189 $$Span = \frac{D_{90} - D_{10}}{D_{50}} \quad \text{eq (1)}$$

190 **2.2.3. Numeric microscopy**

191 Maltodextrin particles were observed thanks to a Dinolite AM73915MZT numeric
192 microscope. A small powder quantity was gently dispersed on a petri dish and was then
193 equilibrated under a range of RH within 30 to 70% and temperature under a range of 20 to 80
194 °C, thanks to a climatic chamber (Climacell, MMM Medcenter, Fisher Bioblock Scientific,
195 Illkirch, France) as described in 2.2.1. Particles morphology was then characterized thanks to
196 microscopy for all conditions and classified as individual particles, caked particles or liquid
197 state. For each maltodextrin powder, 20 conditions were tested in the range 0.3 – 0.7 water
198 activity vs. 20 – 80 °C temperature. For each condition, at least 10 pictures were taken.

199 **2.3. Single particle surface characterization by Atomic Force Microscopy (AFM)**

200 All AFM measurements were performed in air and at 22 ± 2 °C using a Flex-Axiom
201 (Nanosurf, Liestal, Switzerland) with the Nanosurf C3000 controller software.

202 **2.3.1. Sample preparation and single particle selection**

203 Maltodextrins powders were fixed on a circular cover made of borosilicate glass (12 mm
204 radius, 0.13 - 0.17 mm thickness). Powders were gently dispersed on a thin layer of epoxy
205 glue spread on the glass. The samples were left overnight under controlled temperature and
206 RH conditions (as described in 2.2.1.) in order to be in a glassy or rubbery state for AFM

experiments. Single particles were selected for analysis using a micrometer-scale camera mounted on the AFM device.

2.3.2. Surface topography and roughness analysis

Surface topographies were acquired in air thanks to contact mode. The cantilevers used to image the powder surface (Stat0.2LauD cantilevers from Nanosurf, Liestal, Switzerland) have a theoretical spring constant (k_c) of about 0.2 N/m. The scan rate was set at 0.8 s/line. Scanned areas were of 10 µm × 10 µm; 5 µm × 5 µm or 1 µm × 1 µm with a resolution of 256 points × 256 lines. A PID (Proportionnal, Integrative, Derivative) retroaction loop allows to keep constant the cantilever oscillation amplitude. The average surface roughness (Sa) was estimated after levelling AFM images thanks to a second order polynomial filter (Eaton & West, 2010), and was calculated on scanned areas thanks to the **equation 2**.

$$Sa = \frac{1}{n} \sum_{i=1}^{n} |y_i| \qquad \text{eq (2)}$$

where y is the height (z) measured by the piezoelectric scanner at a given pixel (i) in the image. At least 3 images were analyzed to be able to average the surface roughness value.

Finally, height and roughness profiles for a line were extracted from raw data to be able to highlight slight or localized variations on surface roughness (C3000 software, Nanosurf, Liestal, Switzerland).

2.3.3. Mapping nanomechanical properties: Young modulus (E)

AFM nanomechanical properties experiments were performed thanks to cantilevers (DYN190Al-10 cantilevers, Nanosurf, Liestal, Switzerland) with a radius curvature lower than 10 nm. The first step consisted of AFM device calibration before any measurement.

- Spring constant was calculated thanks to the thermal calibration method (Levy & Maaloum, 2002) and was estimated to be about 20-30 N/m.

- Deflection sensitivity also needed to be calibrated with a sample (i.e, glass or silicon) harder than the stiffness of cantilever. This calibration consisted of press and retract movements of the tip on the stiff surface to record five force-distance curves in order to link the cantilever deflection, measured by photodiodes, to the z-axis movement of the scanner. Thus, the displacement gradient of the z-axis piezoelectric scanner related to cantilever deflection allows itself to convert the voltage measured by photodiodes into a reference deflection in nanometer per volts. Generally, this deflection sensitivity was about 80 nm/V and was considered acceptable when the deviation was under 5% (Clifford & Seah, 2005).
- Finally, deflection crosstalk compensation was also calibrated.

To investigate the surface Young modulus of single particles, 1024 force-distance curves were recorded on a grid of 32×32 pixels on a 10 µm ×10 µm area. AFM tip modulation time was set at 250 ms and distance range at 1 µm. Thanks to the previously calculated spring constant, the cantilever deflection can be converted into a force thanks to the Hooke's law (**Equation 3**).

$$F = -k_c \times d \qquad \text{eq (3)}$$

Where F is the Force (N), k_c the cantilever spring constant (N/m) and d the distance (nm). Thus, maximal load at the particle surface was set at 50 nN. All force-distance curves were individually analyzed thanks to the ANA Software (Nanosurf, Liestal, Switzerland). Young modulus (E), also called elastic modulus, was thus analyzed on approach curves using the Hertz Theory for elastic media using conical indenters (Calabri, Pugno, Menozzi, & Valeri, 2008; Cardenas-Perez et al., 2019; Clifford & Seah, 2005; Hertz, 1882) (**Equation 4**).

$$F = \frac{2E \tan\alpha}{\pi\,(1-\upsilon^2)}\,\delta^2 \qquad \text{eq (4)}$$

Where F is the force applied (N), E the Young modulus (Pa), υ the Poisson constant, δ the indentation depth (m) and α the top angle of the tip. Poisson ratio of polymers varies between 0.3 and 0.5. A variation of the Poisson ratio of 0.1 will result in a maximal variation error of the Young modulus value of less than <10% (Dokukin & Sokolov, 2012). Thus, Poisson ratio was set at 0.5, which is the value generally used for AFM indentation on biological samples (Shojaei et al., 2013; Guz, Dokukin, Kalaparthi, Sokolov et al., 2014).

Finally, the analysis of the 1024 approach curves and the Young modulus calculation allow to build highly resolutive elasticity maps. The whole experimental process is summarized in **Figure 1**. At least three elasticity maps were done on independent particles in order to ensure experiment repeatability.

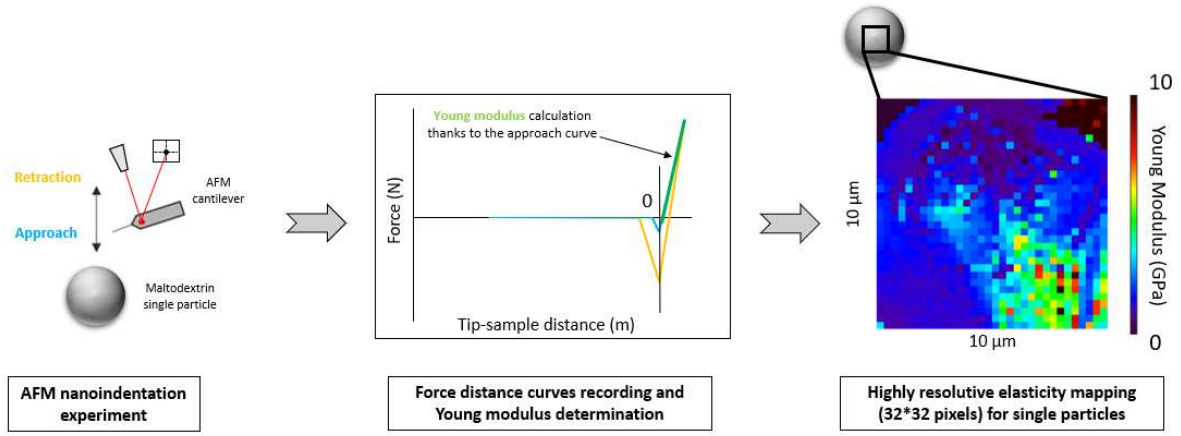

Figure 1. Experimental steps followed to build highly resolutive Young modulus mapping of powder particle surface by AFM

2.4. Powder reconstitution properties

In order to identify the impact of the material (i.e., glass transition phenomenon and DE value) and the stirring rate, the reconstitution ability was measured thanks to a conductimeter (SevenCompact S230, Mettler Toledo, Greifensee, Switzerland) calibrated with a KCl

solution (at 1413 µS/cm). The setup was made up of an agitated and instrumented vessel (250 ml beaker with a magnetic stirrer of 6×20 mm), in which the temperature was controlled and maintained at 25 °C thanks to a thermostated water bath Eco Gold (Lauda, Germany). The conductivity of the solution was followed during the whole reconstitution. This experimental setup was chosen to be in adequation with the standard geometric ratio established by Rushton, Costich, & Everett (1950) and was inspired by Mitchell et al., (2014) and Fournaise, et al., (2021).

Five grams of maltodextrin powder for a final volume of one hundred milliliter were weighed (5% w/v). Shear rate was set at 500, 750, 1 000, 1 250 and 1 500 rpm. Finally, the powder was poured all in once in the instrumented vessel after 10 s and the conductivity was measured every second during the whole reconstitution, allowing to plot reconstitution kinetic curves. Reconstitution was considered as over when the solution reached 90% of its maximal conductivity.

During powder reconstitution, conductivity evolves from an initial value of 0 µS/cm to a final and maximal value which depends on the powder nature. Thus, conductivity values were normalized according to **Equation 5**. (Fournaise et al., 2021) (Gaudel et al., 2022).

$$c\,(t) = \frac{\kappa(t) - k_{ini}}{k_{end} - k_{ini}} \qquad \text{eq (5)}$$

Where c(t) is the normalized conductivity, $\kappa(t)$ the conductivity at a time t, k_{ini} the initial distilled water conductivity and k_{end} the final conductivity. Finally, reconstitution kinetics curves were plot thanks to SigmaPlot (Systat Software Inc, San Jose, California, USA).

2.5. Statistical analyses

292 Statistical analyses were carried out using the OriginPro Software (OriginLab,
293 Northampton, United States). Data were analyzed using a one-way ANOVA and means were
294 compared thanks to the Tukey-HSD test at a level of significance of $p < 0.05$.

295 ## 3. RESULTS AND DISCUSSION

296 ### 3.1. Maltodextrin glass transition

297 For the three maltodextrins, onset Tg values were determined on DSC curves at different
298 beforehand equilibrated a_w (**Appendix A**). **Figure 2** shows that a_w and DE values are two
299 important factors influencing the glass transition for maltodextrin powders. Tg values,
300 whatever the DE, tended to decrease with increased water activity. This phenomenon was
301 attributed to the plasticizing effect of water, which can be modelled using the Gordon-Taylor
302 equation (Roos, 2002; Palzer, 2007). Water increases the molecular mobility of the polymer
303 chains by creating hydrogen bonds. This plasticization phenomenon thus expands the free
304 volume, allowing the overall molecular mobility, leading to a decrease of Tg (Castro et al.,
305 2016; White & Lipson, 2016). Also, a clear tendency of Tg appears related to the DE values.
306 For a given a_w, the Tg value decreases when the DE increases, meaning that maltodextrin
307 molecular weight is directly correlated to the Tg. Maltodextrins with higher DE values exhibit
308 a lower molecular weight distribution and a lower polymer chain length which directly
309 impacts their physical behavior (Avaltroni et al., 2004; Rong et al., 2009; Siemons et al.,
310 2020). Moreover, heating at high temperatures during the DSC measurements did not involve
311 other thermal events on maltodextrins. Castro et al. 2016 also studied the thermal stability of
312 maltodextrins on a large DE value range. A first stage of dehydration was observed within the
313 range of 25 to 150 °C and an onset decomposition temperature around 260 °C for all
314 maltodextrins, meaning that maltodextrins can withstand temperature up to 250 °C.

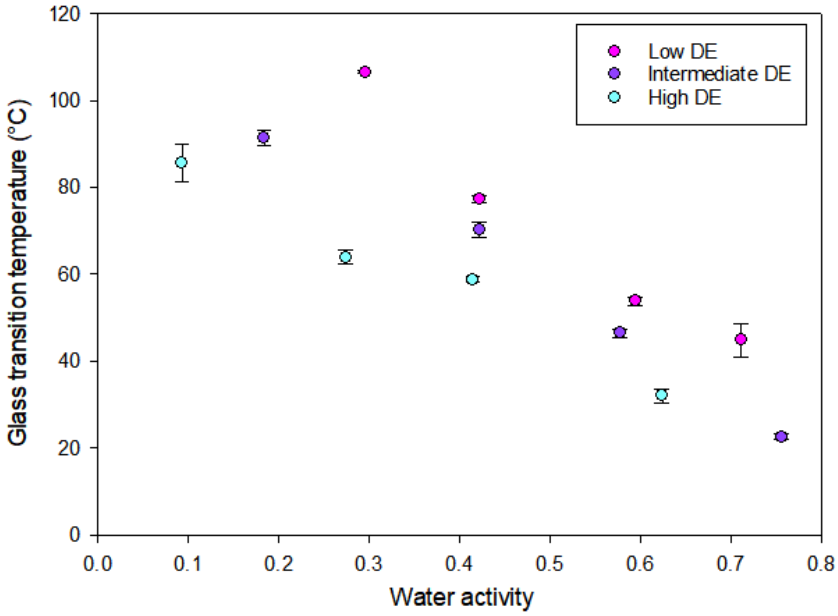

315

316 **Figure 2.** Glass transition onset temperature (T_g) for different maltodextrins depending on their water activity
317 (a_w) represented by the midpoint value

318 However, when the material undergoes glass transition with a_w and/or temperature
319 increase, powders physical properties are impacted. Indeed, maltodextrin particles can be
320 observed as individual or agglomerated particles. They can also be found at the liquid state
321 when the powder is equilibrated at high a_w values. A qualitative map (one for each DE value)
322 of these various material states is displayed in **Figure 3**, which shows particles morphology
323 between 0.3-0.7 a_w and 20-80 °C.

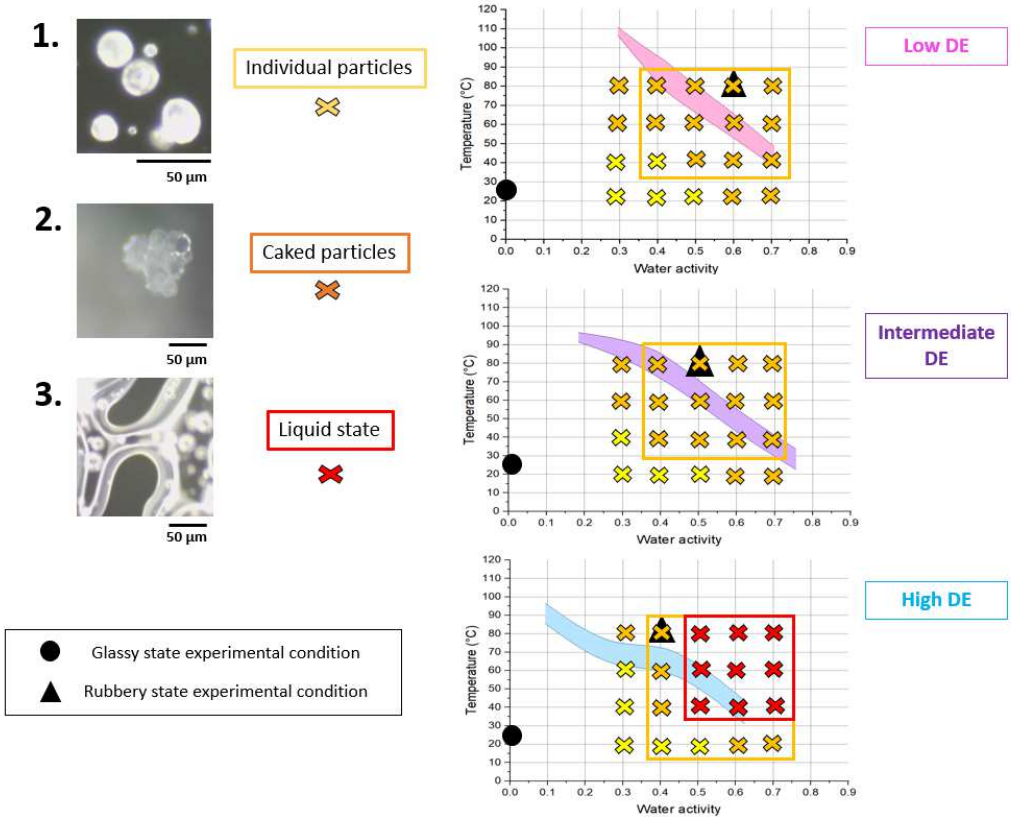

Figure 3. Qualitative map of particle morphology (A. low DE; B. intermediate DE; C. high DE) under controlled temperature and relative humidity conditions observed thanks to numeric microscopy (colored crosses, yellow for individual particles, orange for caked particles and red for liquid state). Particle morphology was checked under each temperature/a_w condition. The glass transition curve is represented by a colored area which is comprised between the Tg onset and endset. Experimental conditions to set powders under the glassy or the rubbery state for the rest of the experiments are identified in the qualitative map as black circle (glassy state) or black triangle (rubbery state).

As it can be highlighted from **Figure 3**, powders are initially well-dispersed. With the increase of a_w, a caking phenomenon is observed and is directly correlated to the glass transition region. In addition to its plasticizing effect, the increase in water activity is somehow correlated to the caking phenomenon, primarily because of the water sensitivity and hygroscopicity. Thus, powders are susceptible to form strong undesired aggregates from the onset of the glass transition, by the formation of liquid then solid bridges, as shown in the study of Descamps et al., (2013) on caking behavior of high DE value maltodextrins. Also, at

very high aw, high DE maltodextrins were found to be at the liquid state, due to the saturation of the powder with water.

Above glass transition temperature, molecular mobility increases critically (Roudaut et al., 2004; Yoshioka & Aso, 2007). Thus, a time-dependent phenomenon of crystallization of low molecular weight components may occur if the powder is under rubbery state conditions, as it is the case of lactose or fructose for example (Roos & Karel, 1992; Roos, 2002; Saavedra-Leos et al., 2014; Wang & Truong, 2017). As maltodextrins are relatively long polymer chains, depending on the DE, they are unlikely subject to crystallization. However, high DE maltodextrins exhibit shorter polymer chains and crystallization of maltose or dextrose only could be possible. Microstructure of different DE values was already detailed in the literature. Thanks to X-ray diffraction, it was shown that diffraction pattern of different DE maltodextrins, at a large range of a_w, shows an amorphous structuration, which remains for all DE and at all the water activities (Saavadra-Leos, Leyva-Porras, Araujo-Diaz, Toxqui-Teran & Borras-Enriquez, 2015). However, to minimize issues encountered at the rubbery state, powder samples need to be stored the nearest possible to the endset region of Tg. As higher DE maltodextrins show lower Tg values, they need to be stored at the lower water activity possible under the rubbery state.

Powders were stored at the experimental conditions described in **Table 1** in order to be in a glassy (i.e., < Tg) or a rubbery state (i.e., > Tg) as presented on qualitative maps into **Figure 3** by a black circle or triangle respectively.

Table 1. Powder storage conditions to keep the powders under a glassy or a rubbery state.

	GLASSY STATE		RUBBERY STATE	
	RH (%)	Temperature (°C)	RH (%)	Temperature (°C)
low DE	0	20	60	80
intermediate DE	0	20	50	80
high DE	0	20	40	80

3.2. Powders reconstitution ability

The reconstitution time was investigated for maltodextrin stored under or above the Tg by following the reconstitution kinetics. Reconstitution times were evaluated by considering the reconstitution as over when conductivity value reaches 90% of its maximal value. Examples of reconstitution kinetic curves, before and after normalization are given in **Appendix B**. **Figure 4** shows that reconstitution times seem to directly depend on the DE value, the powders glassy/rubbery state and the shear rate.

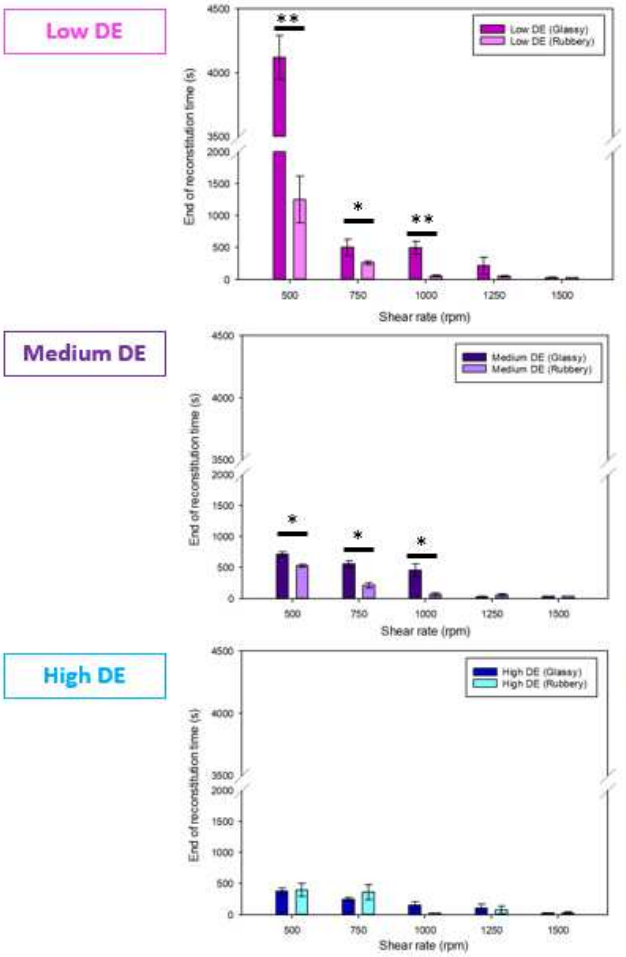

	Glassy state	Rubbery state
500 rpm	4119 ± 171 s	1252 ± 368 s
750 rpm	500 ± 128 s	261 ± 27 s
1000 rpm	495 ± 104 s	55 ± 11 s
1250 rpm	213 ± 131 s	49 ± 10 s
1500 rpm	31 ± 6 s	26 ± 0 s

	Glassy state	Rubbery state
500 rpm	715 ± 37 s	528 ± 25 s
750 rpm	556 ± 51 s	211 ± 45 s
1000 rpm	455 ± 101 s	66 ± 27 s
1250 rpm	32 ± 4 s	56 ± 19 s
1500 rpm	34 ± 0 s	35 ± 2 s

	Glassy state	Rubbery state
500 rpm	377 ± 49 s	397 ± 107 s
750 rpm	245 ± 30 s	360 ± 122 s
1000 rpm	150 ± 58 s	27 ± 2 s
1250 rpm	107 ± 64 s	71 ± 61 s
1500 rpm	25 ± 2 s	29 ± 17 s

Figure 4. Reconstitution times of maltodextrins with different DE values, under glassy or rubbery states and at different shear rates. Statistical analyses were carried out using OriginPro Software using a one-way ANOVA test and Tukey-HSD means comparison method (**: $p \leq 0,01$; *: $p \leq 0,05$).

3.2.1. Impact of the material (DE values and glassy/rubbery state)

373 The reconstitution times observed for the three maltodextrins prove the DE values' crucial
374 role and thus of the molecular weight (**Figure 4**). First, a tendency for faster reconstitution
375 times is observed when the DE values increase whatever the stirring rate and the
376 glassy/rubbery state. This reconstitution improvement is particularly strong between low and
377 intermediate DE values but not significant between intermediate and high DE values. The
378 tendency of shorter reconstitution times with the increase of the DE value is confirmed under
379 the glassy and the rubbery state. That means that lower molecular weight powders (i.e., high
380 DE) tend to reconstitute faster. Thus, the hydrolyzing process upstream of the powder
381 manufacturing is determinant to anticipate the reconstitution of the powder, knowing that
382 maltodextrin powders are derivate products of starch hydrolysis. The first reconstitution step,
383 the wettability, may explain the reconstitution differences observed. Indeed, the powder
384 wettability was observed to be longer when the DE value was lower, as it also shown by the
385 reconstitution kinetics (Appendix C). This observation was supported by Dupas et al., (2017),
386 who studied the contact angle of maltodextrins powders (DE 2, 6 and 29) with water. This
387 later was lower for higher DE value maltodextrins, meaning that low molecular weight
388 maltodextrins should present a better wettability and thus better reconstitution times. Longer
389 reconstitution times for low DE maltodextrins could also be related to the solution viscosity.
390 Low DE maltodextrins solutions are more viscous than those with high DE values. The high
391 viscosity is directly related to the molecular weight (Castro et al., 2016; Dokic, Jakovljevic, &
392 Dokic-Baucal, 1998; Dokic, Jakovljevic, & Dokic, 2004; Siemons et al., 2020, Juszczak,
393 Galkowska, Witczak, & Fortuna, 2013). Knowing that, low DE powders may lead to poor
394 water diffusion between intra and interparticular pores, thus delaying the wetting time and
395 increasing the overall reconstitution time (Ong, Taylor, & Ramaioli, 2020).

396 The impact of glass transition on reconstitution can also be highlighted in **Figure 4**.
397 Reaching the Tg for powders under the rubbery state gives systematically shorter

reconstitution times for low and intermediate DE values. This may be first related to the fact that particle surface is more hydrated, as powders are at higher a_w in the rubbery state, as detailed in experimental conditions defined in **Table 1**. However, this is only true for low and intermediate DE maltodextrins, as differences in the reconstitution times between the glassy and the rubbery state tend to attenuate with higher DE values. Indeed, there are no significant differences in the reconstitution times for high DE powders between the glassy and the rubbery state. To better understand these differences, the impact of particle size should be taken into account. The glass transition is most of the time accompanied by caking, making interparticular forces (such as liquid or solid bridges) stronger. This phenomenon may delay the reconstitution times by the formation of lumps during powder reconstitution, making the dispersion step more difficult (Dupas et al., 2017; Fitzpatrick, 2021; Roos, 2002). In order to see if there is a possible impact of particle size on powders reconstitution time, particle size distribution was evaluated (**Figure 5**).

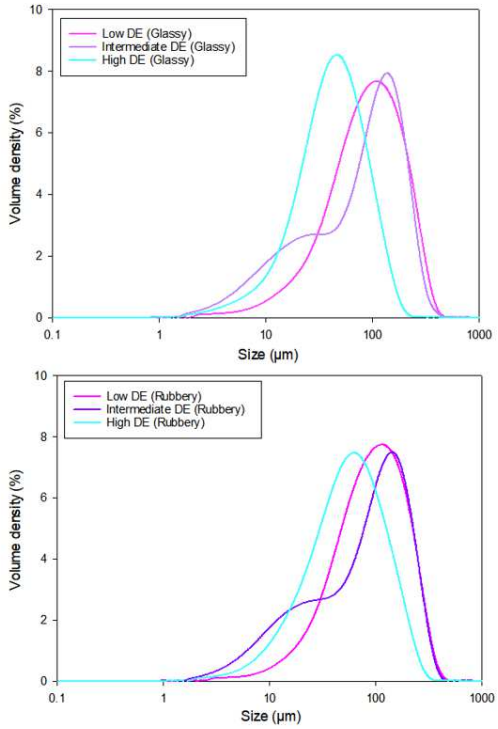

GLASSY STATE	D_{10} (µm)	D_{50} (µm)	D_{90} (µm)	Span
Low DE	27.4 ± 0.7	91.6 ± 2.0	220 ± 2.6	2.10 ± 0.1
Intermediate DE	11.4 ± 0.5	86.7 ± 1.7	204.3 ± 15.3	2.20 ± 0.2
High DE	14.5 ± 0.1	42.5 ± 0.3	204.3 ± 2.1	1.98 ± 0.1

RUBBERY STATE	D_{10} (µm)	D_{50} (µm)	D_{90} (µm)	Span
Low DE	29.5 ± 0.3	93.0 ± 1.4	253.3 ± 43.1	2.0 ± 0.1
Intermediate DE	12.0 ± 0.2	88.7 ± 2.6	271.0 ± 9.0	2.3 ± 0.1
High DE	16.3 ± 0.1	55.2 ± 1.1	142.6 ± 7.2	2.3 ± 0.1

Figure 5. Maltodextrins (low, intermediate, and high DE values) particle size distribution under glassy and rubbery states.

414 It can be highlighted that low and high DE powders presented a monomodal particle size
415 distribution while intermediate DE presented a bimodal distribution. The impact of glass
416 transition on particle size and the width of particle size distribution was only observed for
417 high DE maltodextrins with a D_{50} increase from 42.5 µm to 55.2 µm. No significative
418 differences were found between the glassy and the rubbery state conditions for low and
419 intermediate DE maltodextrins. Therefore, particles size was not directly correlated to both
420 the DE value and the powder glassy or rubbery state. However, those results could explain the
421 reconstitution times obtain at low shear rates, as particle hydration and swelling could be
422 responsible of lumping tendency, especially for low DE maltodextrins, making particles
423 dispersion more difficult, thus making reconstitution longer.

424 **3.2.3. Shear rate effect**

425 Beyond the material effect (i.e. DE values and glassy/rubbery state), the reconstitution time
426 was also directly dependent on the shear rate **(Figure 4)**. The increase of the shear rate from
427 500 to 1500 rpm decreases significantly the reconstitution time whatever the powder. For
428 example, the reconstitution time decreases 99% under the glassy state and 97% under the
429 rubbery state for low DE powders and it varies in the same way for the other DE value
430 maltodextrins. These results agree with those in the literature, describing that high shear rate
431 allows logically shorter reconstitution times, and is also useful to prevent lump formation or
432 sedimentation, especially for maltodextrins powders (Mitchell et al., 2014). Differences
433 between the reconstitution times for all maltodextrins tend to attenuate with the increase of
434 the solution stirring. Indeed, high shear rates allow instant reconstitution properties, whatever
435 the powder. However, a high variability for the reconstitution time is noticed at high shear
436 rates (1250 rpm), as it is particularly the case for high DE maltodextrins in the rubbery state
437 and to a lesser extent in the glassy state.

Also, the shear rate seems to improve the reconstitution time, but the impact is not the same depending on the material's physical state. Until now, only a few works accurately describe the effect of both shear rate and powder physical state on reconstitution. Gaudel et al., (2022) studied the impact of the glass transition on different fruit-based powders and highlighted that reconstitution rate was impacted by the powder physical state. They observed that fruits powders under the glassy state were shear rate dependent, while the same powders under a rubbery state were shear rate independent. A viscous layer was formed at the particle surface for powders under a rubbery state, preventing water from diffusing. Our results are in agreement with this study as maltodextrin powders under the glassy state were found more shear rate dependent than powders under the rubbery state. Nevertheless, shear rate differences between glassy and rubbery powders reconstitution times were attenuated by the increase of DE, showing its strong impact.

All these results agree with the role of the powder physical (glassy/rubbery) and chemical (DE values) properties on reconstitution. In particular, the shear rate applied to reconstitute the powders was found to have a greater impact when the material is under the glassy state, meaning that increasing stirring improves reconstitution properties. The results also highlighted that wetting seems to be a determining step of powders reconstitution behavior at low shear rates, especially for maltodextrins (Dupas et al., 2017).

3.3. Probing single particle surface properties by Atomic Force Microscopy (AFM)

AFM is a powerful and resolutive tool to analyze the surface of food powders. This technique is also very versatile as it allows to characterize with a nanoscale precision the surface topography, its roughness and the nanomechanical properties of single particles (Burgain et al., 2017; Murrieta-Pazos et al., 2012).

3.3.1. Surface topography and roughness analysis

462 AFM topographies and their associated height profiles performed under the glassy or
463 rubbery states on single maltodextrins particles are displayed in **Figure 6**.

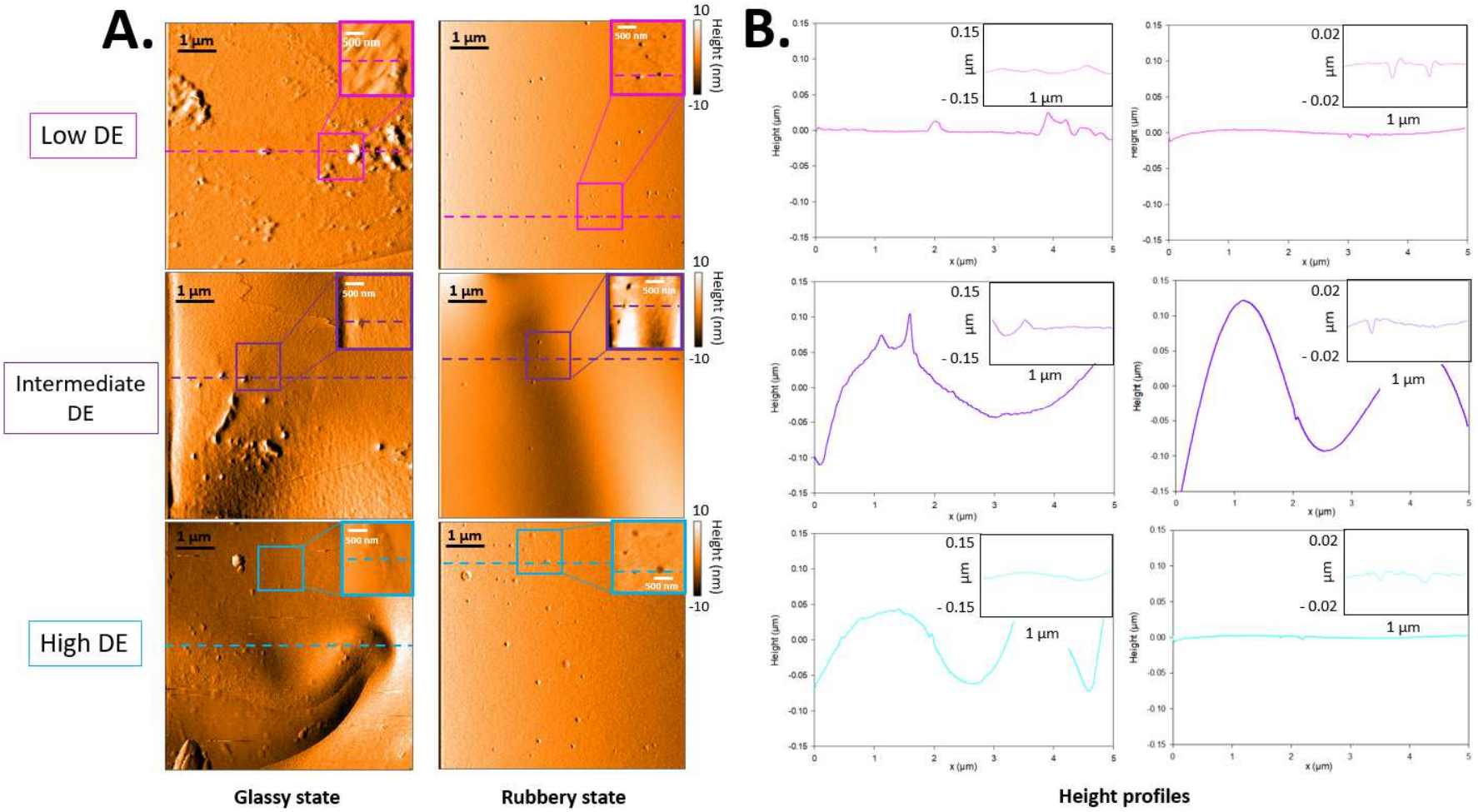

Figure 6. A. AFM deflection views of all maltodextrins under glassy (left) or rubbery (right) experimental conditions. B. Height profiles under glassy (left) or rubbery (right) states associated to the previous topographies. Dash lines in A. are corresponding to the height profiles extracted from raw data in B.

Powders surface topography seem to be directly correlated to the DE value, especially when they are under the glassy state **(Figure 6A)**. By taking a closer look at the height profiles of powders under the glassy state, increasing the DE value makes the surface more levelled with a lot of irregularities (**Figure 6B**). Thus, low DE maltodextrins appear to have a more regular surface and smooth than higher DE maltodextrins. To highlight the effect of the DE values on surface topography, the average surface roughness (Sa) was calculated on 10 × 10 µm scanned areas, according to **Equation 2**. Extracted roughness profiles from acquired images are also displayed in **Figure 7A**.

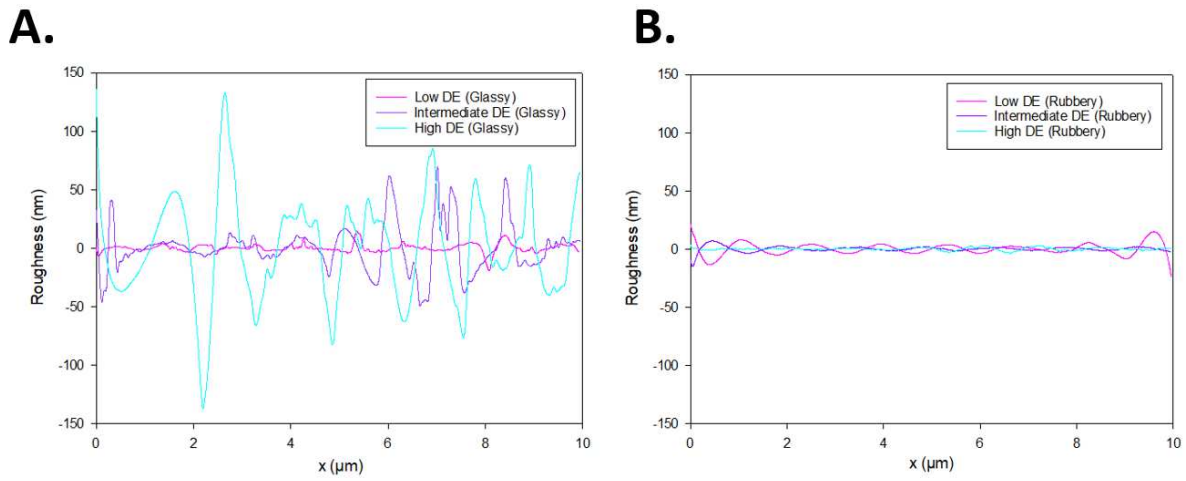

Figure 7. Low, intermediate, and high DE maltodextrins roughness profiles under the glassy (A.) or rubbery (B.) state experimental conditions

Thus, low DE maltodextrins were the ones with the lowest estimated average surface roughness value (Sa = 12.36 ± 5.59 nm) under a glassy state. Then, a localized increase in the surface roughness was observed for intermediate DE maltodextrins (Sa = 79.09 ± 26.56 nm) followed by high DE maltodextrins (Sa = 128.83 ± 25.36 nm). That means that the more the maltodextrin is hydrolyzed, the higher the global overall particle surface roughness will be. Thanks to SEM, Takeiti et al. (2010) evidenced the effect of the botanical source and the drying process conditions on the size and shape of produced maltodextrin powders. Siemons et al. (2020) highlighted the effect of the DE value on the particle morphology in a single

sessile droplet drying. Low DE value maltodextrins were generally smoothly shaped particles with large cavities. The opposite can be observed for high DE value maltodextrins presenting many surface irregularities. Here, for the first time, AFM was used to evidence localized variations of the surface roughness of maltodextrins correlated to their DE value, showing that high DE value maltodextrins exhibit a much more irregular surface than those by a lower DE value. These variations on particles surface topographies could also explain the better reconstitution times observed at low shear rates for high DE value maltodextrins compared to lower ones **(Figure 4)**. An increase of the overall surface roughness at the particle surface could enhance the contact with water, by increasing the surface area in contact with the reconstitution media, thus allowing shorter reconstitution times. On the best knowledge of authors, the effect of surface roughness on reconstitution properties is poorly described in the literature. A few studies detailing how roughness can influence contact with water were reported on other food materials, such as spaghettis. Their rehydration kinetics were improved by altering the overall surface roughness by the use of different dies during manufacturing. It was shown that low surface roughness materials had longer rehydration times compared to higher surface roughness materials, meaning that measuring roughness was relevant when it comes to reconstitution kinetics, as it could be an enhancer of contact with water (Ogawa & Adachi, 2014, Ogawa & Adachi, 2017).

The impact of glass transition on single-particle topography and surface roughness can also be highlighted **(Figure 6) (Figure 7B)**. The surface appears much smoother when the material is rubbery than when it is in the glassy state. Average surface roughness was estimated to be 8.70 ± 2.30 nm for low, 6.19 ± 5.34 nm for intermediate and 7.82 ± 4.45 nm for high DE values. This surface smoothing observed under the rubbery state could be explained by the increased water adsorbed as a thin layer at the particle surface, when powders are exposed to high relative humidity. These results could also be related to the reconstitution times (**Figure**

511 **4**). Improved reconstitution times were observed under the rubbery state due to a more
512 hydrated surface layer. This enhanced the powder wettability, thus allowing lower
513 reconstitution times, except for high DE maltodextrins.

514 In addition to the overall surface smoothing, the glass transition was accompanied by the
515 formation of slight hollow zones of about 3 to 10 nm, as shown in **Figure 6**. This kind of
516 hollow area, which seems to appear randomly, could be related to water adsorption at the
517 particle surface followed by a swelling phenomenon. Indeed, the swelling observed by
518 Deslandes et al., (2019) for carbohydrates polymers at a temperature range within 60 to 80 °C
519 corresponds to the experimental conditions used in this work **(Table 1)**.

520 **3.3.2. Mapping single particles nanomechanical properties**

521 Another use of AFM is the analysis of the Young modulus at the particle surface by the
522 generation of elasticity mapping, giving information about single particles nanomechanics.
523 Elasticity mapping and associated distribution histograms of all maltodextrins are displayed in
524 **Figure 8.**

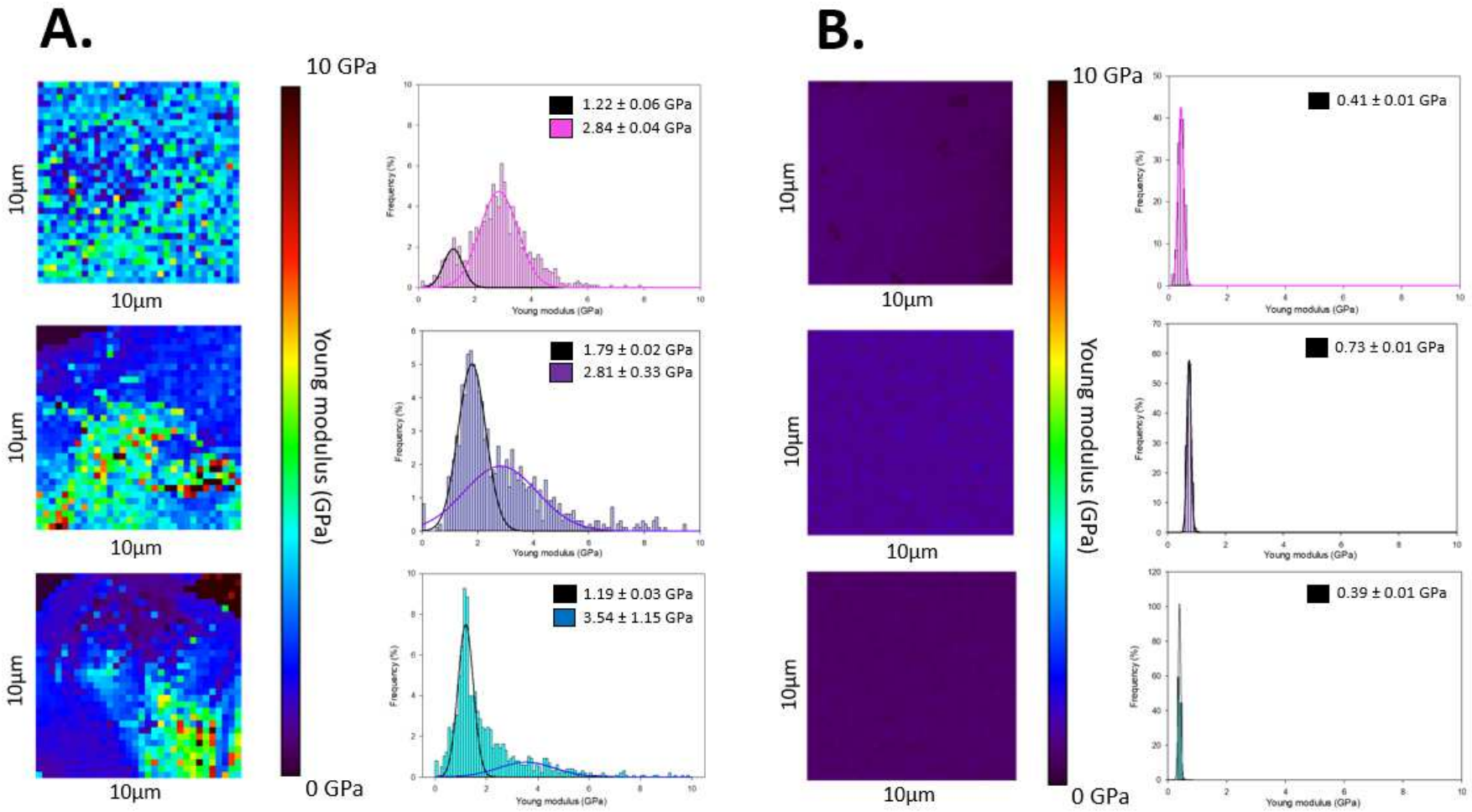

525

526 **Figure 8.** Young modulus mapping (10×10 µm) and associated distribution histograms for maltodextrin single particles. A. under a glassy state and B. under a rubbery state

527 (Up: low DE; middle: intermediate DE; bottom: high DE)

In the glassy state, all maltodextrins show two Young modulus populations **(Figure 8A)** with a distribution rather scattered and presenting nanoscale slight variations. Glassy state maltodextrins exhibit two Young modulus populations with a gaussian distribution. Thus, low DE maltodextrins modulus distribution was calculated at 1.22 ± 0.06 GPa for the first population and 2.84 ± 0.04 GPa for the second one. In the same way, modulus of intermediate DE maltodextrins was estimated at 1.79 ± 0.02 GPa and 2.81 ± 0.33 GPa and was about 1.19 ± 0.03 GPa and 3.54 ± 1.15 GPa for high DE maltodextrins. The presence of two Young modulus populations with harder regions could not be first related to crystallized areas, as crystallization is unlikely for maltodextrins. This could maybe be explained by a low range of molecular association between polymer chains, similar to starch retrogradation. Indeed, retrogradation is induced at low temperatures and is dependent on the molecular weight. During this event, association of different molecular weight polymer chain occurs and intermolecular distance decreases, leading to a water removal (Karim, Norziah, & Seow, 2000; Sobolewska-Zielinska & Fortuna, 2010). This could lead to the creation of pockets with lower moisture content and which show a higher Young modulus, explaining the nanoscale variation of the Young modulus.

Up to now, nanoindentation studies have been mostly performed on pharmaceutical powders which contain various carbohydrates as excipients. Masterson and Cao, (2008) report a better understanding of the mechanical properties of complex pharmaceutical powders with the characterization of the modulus of crystalline sucrose and lactose single particles. They found that the hardness value varies from 1.8 to 2.4 GPa for crystalline sucrose particles and from 0.18 to 0.51 GPa for lactose particles. Only few authors used AFM to assess the nanomechanical properties of food powders. Burgain et al., (2016b) investigated rehydration impairments linked to the surface hardening of micellar casein powders depending on storage conditions, especially temperature. The Young modulus of fresh casein powders was

553 estimated at 0.2 GPa whereas it was about 20 GPa for aged casein powders. Haider et al.,
554 (2013) characterized the Young modulus of glassy DE 21 maltodextrins. They found a
555 modulus value of 3.34 ± 1.1 GPa, which is relatively close to the values obtain in this work.

556 Elasticity mapping and modulus histograms distribution of the different maltodextrins in
557 rubbery state are displayed in **Figure 8B**. As shown, powders Young modulus value are of
558 0.41 ± 0.01 GPa for low DE, 0.73 ± 0.01 GPa for intermediate DE and 0.39 ± 0.01 GPa for
559 high DE maltodextrins. A large decrease of the Young modulus at the surface of the
560 maltodextrin particle can be observed. Moreover, a single Gaussian population is observed,
561 meaning that the elasticity distribution at the surface becomes less dispersed and more
562 homogenous. Particles under a rubbery state are thus softer because of a hydrated surface
563 layer. Already existing water adsorption at the particle surface, explaining the decrease of the
564 surface hardness and the initiation of the wetting step for particles under a rubbery state.

565 **Table 2**. Summary of the results presented in this work, showing the direct link between material physical state,
566 from macro- to microscale and reconstitution properties.

567

Maltodextrin powders (low/intermediate/high DE values)	Glassy state	Rubbery state
Macroscale properties		
Glass transition temperature	• Tg decreases with the increase of the DE value (i.e., decreasing polymer chain length) • Increasing water content leads to a decrease of Tg (plasticizing effect)	
Reconstitution time	• Reconstitution strongly shear rate dependent	• Reconstitution poorly shear rate dependent
	• Better reconstitution times for high DE values • Better reconstitution times when maltodextrin is under the rubbery state • Differences in reconstitution times between glassy and rubbery states are attenuated for high DE values	
Mesoscale / Microscale properties		
Particle size	• All maltodextrins present the same particle size	• Slight particle size increase due to water adsorption at the surface
Particle surface	• Rough particles	• Smooth particles and low

568

topography	• Increase of surface roughness with the DE values	surface roughness • Formation of nanoscale hollows structures
Young modulus	• High Young modulus • Bimodal distribution with harder points (related to lower moisture content regions)	• Low Young modulus • Homogenous distribution

4. CONCLUSION

This work evaluated the reconstitution properties of maltodextrin powders depending on their physical state **(Table 2)**. To characterize the material properties, Tg of different maltodextrins were first determined, and Tg was found dependent on both the maltodextrin molecular weight and a_w. Also, powder reconstitution times under the glassy state were mostly shear rate and DE dependent, with better reconstitution times while increasing these two parameters. On the contrary, the reconstitution properties of powders under the rubbery state were less shear rate and DE dependent with better reconstitution times while increasing these two parameters. Particle surface properties were also analyzed by AFM, which has been yet poorly used on food powders. Particles under a glassy state were relatively rough and hard with a lot of surface irregularities, whereas powders under a rubbery state were much smoother and softer. The decrease of the Young modulus under the rubbery state was also related to a more hydrated surface, which enhanced the wetting step. Finally, nanoscale hollows formation was highlighted for particles under the rubbery state. The correct management of powder reconstitution needs to consider powder macroscopic properties (granulometry, Tg, chemical composition) which are related to surface microscopic features (roughness, elasticity, hygroscopicity). In this work the interplay between the two measurement scale is described for maltodextrin powders and can be henceforward applied to other food powders.

5. Acknowledgements

589 The authors acknowledge financial support from the "Impact Biomolecules" project of the
590 "Lorraine Université d'Excellence" (in the context of the « Investissements d'avenir »
591 program implemented by the French National Research Agency (ANR 15-004)).

592 6. References

593 Arora, S., Kappl, M., Haghi, M., Young, P.M., Traini, D., & Jain, S., (2016).
594 Investigation of surface properties, local elastic modulus and interaction with simulated
595 pulmonary surfactant of surface modified inhalable voriconazole dry powders using atomic
596 force microscopy. *RSC Advances*, 6 (31), 25789-25798. https://doi.org/10.1039/C6RA01154C

597 Avaltroni, F., Bouquerand, P.E., & Normand, V., (2004). Maltodextrin molecular
598 weight distribution influence on the glass transition temperature and viscosity in aqueous
599 solutions. *Carbohydrate Polymers*, 58, 323-334.
600 http://dx.doi.org/10.1016/j.carbpol.2004.08.001

601 Barringer, S., (2013). Coating foods with powders. In B. Bhandari, N. Bansal, M.
602 Zhang, P. Schuck (Eds.), *Handbook of Foods Powders* (pp. 625-640).
603 http://dx.doi.org/10.1533/9780857098672.3.625

604 Berard, V., Lesniewska, E., Andres, C., Pertuy, D., Laroche, C., & Pourcelot, Y.,
605 (2002). Dry powder inhaler: influence of humidity on topology and adhesion studied by AFM.
606 *International journal of Pharmaceutics*, 232 (1-2), 213-224. http://dx.doi.org/10.1016/S0378-
607 5173(01)00913-9

608 Bhandari, B., (2013). Introduction to food powders. In B. Bhandari, N. Bansal, M.
609 Zhang, P. Schuck (Eds.), *Handbook of Foods Powders* (pp. 1-25).

610 Burgain, J., El Zein, R., Scher, J., Petit, J., Norwood, E.A., Francius, G., & Gaiani, C.,
611 (2016a). Local modification of whey protein isolate powder surface during high temperature
612 storage. *Journal of Food Engineering*, 178, 39-46.
613 https://dx.doi.org/10.1016/j.jfoodeng.2016.01.005

614 Burgain, J., Scher, J., Petit, J., Francius, G., & Gaiani, C., (2016b). Links between
615 particle surface hardening and rehydration impairment during micellar casein powder storage.
616 *Food Hydrocolloids*, 61, 277-285. https://doi.org/10.1016/j.foodhyd.2016.05.021

617 Burgain, J., Petit, J., Scher, J., Rasch, R., Bhandari, B., & Gaiani, C., (2017). Surface
618 chemistry and microscopy of food powders. *Progress in Surface Science*, 92 (4), 409-429.
619 DOI https://doi.org/10.1016/j.progsurf.2017.07.002

620 Butt, H.-J., Cappella, B., & Kappl, M., (2005). Force measurements with the atomic
621 force microscope: Technique, interpretation and applications. *Surface Science Reports*, 59, 1-
622 152. https://doi.org/10.1016/j.surfrep.2005.08.003

623 Calabri, I., Pugno, N., Menozzi, C., & Valeri, S., (2008). AFM nanoindentation: tip
624 shape and tip radius of curvature effect on the hardness measurement. *Journal of Physics:*
625 *Condensed Matter*, 20. http://dx.doi.org/10.1088/0953-8984/20/47/474208

626 Cardenas-Perez, S., Chanona-Perez, J.J., Mendez-Mendez, J.V., Arzate-Vazquez, I.,
627 hernandez-Varela, J.D., & Guemes Vera, N., (2019). Recent advances in atomic force

microscopy for assessing the nanomechanical properties of food materials. *Trends in Food Sciences & Technology*, 87, 59-72. https://doi.org/10.1016/j.tifs.2018.04.011

Castro, N., Durrieu, V., Raynaud, C., & Rouilly, A., (2016). Influence of DE-value on the physicochemical properties of maltodextrin for melt extrusion processes. *Carbohydrate Polymers*, 144, 464-473. https://doi.org/10.1016/j.carbpol.2016.03.004

Chronakis, I.S., (1998). On the molecular Characteristics, Compositional Properties, and Structural-Functional Mechanisms of Maltodextrins: A Review. *Critical Reviews in Food Science and Nutrition*, 38 (7), 599-637. https://doi.org/10.1080/10408699891274327

Clifford, C.A., & Seah, M.P., (2005). Quantification issues in the identification of nanoscale regions of homopolymers using modulus measurement via AFM nanoindentation. *Applied Surface Sciences,* 252, 1915-1933. https://doi.org/10.1016/j.apsusc.2005.08.090

Crowley, S.V., Kelly, A.L., Schuck, P., Jeantet, R., & O'Mahony, J.A., (2016). Rehydration and solubility characteristics of high protein dairy powders. In P.L.H. McSweeney, J.A. O'Mahony (Eds.), *Advanced Dairy Chemistry* (pp. 99-131).

Cuq, B. & Mandato, S., (2013). Agglomeration/granulation in food powder production. In B. Bhandari, N. Bansal, M. Zhang, P. Schuck (Eds.), *Handbook of Foods Powders* (pp. 150-177).

Descamps, N., Palzer, S., Roos, Y.H., & Fitzpatrick, J.J., (2013). Glass transition and flowability/caking behavior of maltodextrin DE 21. *Journal of Food Engineering*, 119, 809-813. http://dx.doi.org/10.1016/j.jfoodeng.2013.06.045

Deslandes, F., Plana-Fattori, A., Almeida, G., Moulin, G., Doursat, C., & Flick, D., (2019). Estimation of individual starch granule swelling under hydro-thermal treatment. *Food Structure*, 22, 100-125. https://doi.org/10.1016/j.foostr.2019.100125

Dokic, P., Jakovljevic, J., & Dokic-Baucal, Lj., (1998). Molecular characteristics of maltodextrins and rheological behaviour of diluted and concentrated solutions. *Colloids and Surface A: Physicochemical and Engineering Aspects*, 141, 435-440. https://doi.org/10.1016/S0927-7757(97)00118-0

Dokic, L., Jakovljevic, J., & Dokic, P., (2004). Relation between Viscous Characteristics and Dextrose Equivalent of Maltodextrins. *Starch*, 56 (11), 520-525. https://doi.org/10.1002/star.200400294

Dokukin, M. & Sokolov, I., (2012). On the measurements of Rigidity Modulus of Soft Materials in Nanoindentation Experiments at Small Depth. *Macromolecules*, 45 (10), 4277-4288). https://doi.org/10.1021/ma202600b

Dufrene, Y.F., (2002). Atomic Force Microscopy, a Powerful Tool in Microbiology. *Journal of Bacteriology*, 184 (19), 5205-5213. https://doi.org/10.1128/JB.184.19.5205-5213.2002

Dupas, J., Girard, V., & Forny, L., (2017). Reconstitution properties of Sucrose and Maltodextrins. *Langmuir*, 33, 988-995. https://doi.org/10.1021/acs.langmuir.6b04380

Eaton, P. & West, P., (2010). *Atomic Force Microscopy*, Oxford University Press.

Fitzpatrick, J.J., Hodnett, M., Twomey, M., Cerqueira, P.S.M., O'Flynn, J., & Roos, Y.H., (2007). Glass transition and the flowability and caking of powders containing

amorphous lactose. *Powder Technology*, 178, 119-128. https://doi.org/10.1016/j.powtec.2007.04.017

Fitzpatrick, J.J., van Lauwe, A., Coursol, M., O'Brien, A., Fitzpatrick, K.L., Ji, J., & Miao, S., (2016). Investigation of the rehydration behaviour of food powders by comparing the behaviour of twelve powders with different properties. *Powder Technology*, 297, 340-348, https://doi.org/10.1016/j.powtec.2016.04.036

Fitzpatrick, J.J., Ji, J., & Miao, S., (2021). Characterisation of the Rehydration Behaviour of Food Powders. *Food Powders Properties and Characterization*, 91-108. http://dx.doi.org/10.1007/978-3-030-48908-3_5

Forny, L, Marabi, A., & Palzer, S., (2011). Wetting, disintegration and dissolution of agglomerated water-soluble powders. *Powder Technology*, 206, 72-78. https://doi.org/10.1016/j.powtec.2010.07.022

Fongin, S., Kawai, K., Harnkarnsujarit, N., & Hagura, Y., (2017). Effects of water and maltodextrin on the glass transition temperature of freeze-dried mango pulp and an empirical model to predict plasticizing effect of water on dried fruits. *Journal of Food Engineering*, 210, 91-97. http://dx.doi.org/10.1016/j.jfoodeng.2017.04.025

Fournaise, T., Petit, J., & Gaiani, C., (2021). Main powder physicochemical characteristics influencing their reconstitution behavior. *Powder Technology*, 383, 66-73. DOI https://doi.org/10.1016/j.powtec.2021.01.056

Frascareli, E.C., Silva, V.M., Tonon, R.V., & Hubinger, M.D., (2012). Determination of critical storage conditions oil microcapsule by coupling water sorption isotherms and glass transition temperature. *International Journal of Food Science and Technology*, 47 (5), 1044-1054. http://dx.doi.org/10.1111/j.1365-2621.2012.02939.x

Gaboriaud, F., & Dufrene, Y.F., (2007). Atomic force microscopy of microbial cells: Application to nanomechanical properties, surface forces and molecular recognition forces. *Colloids Surface B: Biointerfaces,* 54, 10-19. https://doi.org/10.1016/j.colsurfb.2006.09.014

Gaiani, C., Scher, J., Ehrhardt, J.J., Linder, M., Schuck, P., Desobry, S., Banon, S., & (2007a). Relationships between Dairy Powder Surface Composition and Wetting Properties during Storage: Importance of Residual Lipids. https://doi.org/10.1021/jf070364b

Gaiani, C., Schuck, P., Scher, J., Desobry, S., Banon, S., (2007b). Dairy Powder Rehydration: Influence of Protein State, Incorporation Mode, and Agglomeration. *Journal of Dairy Science*, 90 (2), 570-581. https://doi.org/10.3168/jds.S0022-0302(07)71540-0

Gaiani, C., Burgain, J., & Scher, J., (2013). Surface composition of food powders. In B. Bhandari, N. Bansal, M. Zhang, P. Schuck (Eds.), *Handbook of Foods Powders* (pp. 339-378). https://dx.doi.org/10.1533/9780857098672.2.339

Gaudel, N., Gaiani, C., Harshe, Y.M., Kammerhofer, J., Pouzot, M., Desobry, S., & Burgain, J., (2022). Reconstitution of fruit powders: A process-structure-function approach. *Journal of Food Engineering*, 315. https://doi.org/10.1016/j.jfoodeng.2021.110800

Guz, N., Dokukin, M., Kalaparthi, V., Sokolov, I., (2014). If Cell Mechanics Can Be Described by Elastic Modulus: Study of Different Models and Probes Used in Indentation Experiments. *Biophysical Journal*, 107 (3), 564-575. https://doi.org/10.1016/j.bpj.2014.06.033

Haider, C.I., Althaus, T.O., Niederreiter, G., Palzer, S., Hounslow, M.J., & Salman, A.D., (2013, June). *Elastic behavior of glassy cohesive maltodextrin in particle contact experiments*. Paper presentation for the 6th International Granulation Workshop, Sheffield, UK.

Hertz, H., (1882). Uber die Berührung fester elasticher Körper. https://doi.org/10.1515/crll.1882.92.156

Islam, I.-U., & Langrish, T.A.G., (2013). Modelling crystallization in spray-drying for food powder production. In B. Bhandari, N. Bansal, M. Zhang, P. Schuck (Eds.), *Handbook of Foods Powders* (pp. 105-131)

Juszczak, L., Galkowska, D., Witczak, T., & Fortuna, T., **(2013)**. Effect of Maltodextrins on the Rheological Properties of Potato Starch Pastes and Gels. *International Journal of Food Science*, 2013, 1-7. https://doi.org/10.1155/2013/869362

Karim, A.A., Norziah, M.H., & Seow, C.C., (2000). Methods for the study of starch retrogradation. *Food Chemistry*, 71, 9-36. https://doi.org/10.1016/S0308-8146(00)00130-8

Kong, F. & Singh, R.P., (2016). Chemical Deterioration and Physical Instability of Foods and Beverages. In P. Subramaniam (Eds.), *The stability and Shelf Life of Food* (pp. 43-76). http://dx.doi.org/10.1016/B978-1-84569-701-3.50002-5

Levy, R., & Maaloum, M., (2001). Measuring the spring constant of atomic force microscope cantilevers: thermal fluctuations and other methods. *Nanotechnology*, 13 (1), 33. http://dx.doi.org/10.1088/0957-4484/13/1/307

Li, K., Pan, B., Ma, L., Miao, S., & Ji, J., (2020). Effect of Dextrose Equivalent on Maltodextrin/Whey Protein Spray-Dried Powder Microcapsules and Dynamic Release of Loaded Flavor during Storage and Powder Rehydration. *Foods*, 9 (12), 1878. https://doi.org/10.3390/foods9121878

Liao, X., & Wiedmann, T.S., (2003). Characterization of Pharmaceutical Solids by Scanning Probe Microscopy. *Journal of Pharmaceutical Sciences*, 93 (9), 2250-2258. https://doi.org/10.1002/jps.20139

Masterson, V.M., & Cao, X., (2008). Evaluating particle hardness of pharmaceutical solids using AFM nanoindentation. *International Journal of Pharmaceutics*, 262, 163-171. https://doi.org/10.1016/j.ijpharm.2008.06.015

Mitchell, W.R., Forny, L., Althaus, T.O., Niederreiter, G., Palzer, S., Hounslow, M.J., & Salman, A.D., (2014). Mapping the rate-limiting regimes of food powder reconstitution in a standard mixing vessel. *Powder Technology*, 270, 520-527. https://doi.org/10.1016/j.powtec.2014.08.014

Murrieta-Pazos, I., Gaiani, C., Galet, L., Cuq, B., Desobry, S., & Scher, J., (2011). Comparative study of particle structure evolution during water sorption: Skim and whole milk powders. *Colloids and Surface B: Biointerfaces*, 87 (1), 1-10. https://doi.org/10.1016/j.colsurfb.2011.05.001

Murrieta-Pazos, I., Gaiani, C., Galet, L., Calvet, R., Cuq, B., & Scher, J., (2012). Food powders: Surface and form characterization revisited. *Journal of Food Engineering*, 112, 1-21. https://dx.doi.org/10.1016/j.jfoodeng.2012.03.002

752 Ogawa, T., Adachi, S., (2014). Effect of surface roughness on rehydration kinetics of
753 spaghetti. *Japan Journal of Food Engineering*, 15 (2), 101-104.
754 http://dx.doi.org/10.11301/jsfe.15.101

755 Ogawa, T., & Adachi, S., (2017). A Simple Method to Measure the Surface Roughness
756 of Spaghetti Using a Digital Camera. *Food Science and Technology Research*, 2, 237-240.
757 https://doi.org/10.3136/fstr.23.237

758 Ong, X.Y., Taylor, S.E., & Ramaioli, M., (2020). Rehydration of food powders:
759 Interplay between physical properties and process conditions. *Powder Technology*, 371, 142-
760 153. https://doi.org/10.1016/j.powtec.2020.05.066

761 Palzer, S., (2007). Agglomeration of Dehydrated Consumer Foods. In A.D. Salman, M.
762 Ghadiri, & M.I. Hounslow (Eds.) *Handbook of Food Technology* (pp. 592-671).
763 https://doi.org/10.1016/S0167-3785(07)80048-0

764 Perkins, M., Ebbens, S.J., Hayes, S., Roberts, C.J., Madden, C.E., & Luk, S.Y., (2007).
765 Elastic modulus measurements from individual lactose particles using atomic force
766 microscopy. *International Journal of Pharmaceutics*, 332 (1), 168-175.
767 https://doi.org/10.1016/j.ijpharm.2006.09.032

768 Prime, D.C., Stapley, A.G.F., Rielly, C.D., Jones, J.R., & Leaper, M.C., (2011a).
769 Analysis of Powder Caking in Multicomponent Powders Using Atomic Force Microscopy to
770 Examine Particle Properties. *Chemical Engineering and Applied Chemistry*, 34, 1, 98-102.
771 https://doi.org/10.1002/ceat.201000211

772 Prime, D.C., Leaper, M.C., Jones, J.R., Richardson, D.J., Rielly, C.D., & Stapley,
773 A.G.F., (2011b). Caking Behaviour Of Spray-Dried Powders - Using Scanning Probe
774 Microscopy to Study Nanoscale Surface Properties and Material Composition. *Chemical*
775 *Engineering and Applied Chemistry*, 34 (7), 1104-1108.
776 http://dx.doi.org/10.1002/ceat.201000537

777 Ramos, K.J. & Bahr, D.F., (2007). Mechanical behavior assessment of sucrose using
778 nanoindentation. *Journal of Material Research*, 22 (7), 2037-2045.
779 https://doi.org/10.1557/jmr.2007.0249

780 Ratti, C., (2013). Freeze drying for food powder production. In B. Bhandari, N. Bansal,
781 M. Zhang, P. Schuck (Eds.), *Handbook of Foods Powders* (pp. 57-84)

782 Rong, Y., Sillick M., & Gregson, C.M., (2009). Determination of Dextrose Equivalent
783 Value and Number Average Molecular Weight of Maltodextrin by Osmometry. *Journal of*
784 *Food Science*, 74 (1), 33-40. https://doi.org/10.1111/j.1750-3841.2008.00993.x.

785 Roos, Y., & Karel, Y., (1992). Crystallization of Amorphous Lactose. *Journal of Food*
786 *Science*, 57 (3), 775-777. https://doi.org/10.1111/j.1365-2621.1992.tb08095.x

787 Roos, Y.H., (2002). Importance of glass transition and water activity to spray-drying
788 and stability of dairy powders. *Le lait, INRA Editions*, 82 (4), 475-484.
789 https://doi.org/10.1051/lait:2002025

790 Roos, Y.H., (2006). Phase Transitions and Transformations in Food Systems. In D.R.
791 Heldman & D.B. Lund, (Eds.), *Handbook of Food Engineering* (2nd ed.) (pp. 288-346)

792 Roos, Y.H. & Drusch, S., (2016). Introduction to phase transitions. In Y.H., Roos & S.
793 Drusch (Eds.), *Phase Transitions in Foods (2nd Edition*) (pp 1-17)

794 Roudaut, G., Simatos, D., Champion, D., Contreras-Lopez, E., Le Meste, M., (2004).
795 Molecular mobility around the glass transition temperature: a mini review. *Innovative Food*
796 *Science & Emerging Technologies*. https://dx.doi.org/10.1016/j.ifset.2003.12.003

797 Rushton, J., Costich, E., & Everett, H., (1950). Power characteristics of mixing
798 impellers. *Chemical Engineering Progress*, 46, 395–476.

799 Saavedra-Leos, M.Z., Leyva-Porras, C., Martinez-Guerra, E., Pérez-Garcia, S.A.,
800 Aguilar-Martinez, J.A., Alvarez-Salas, C., (2014). Physical properties of inulin and inulin-
801 orange juice: Physical characterization and technological application. *Carbohydrate*
802 *Polymers*, 105, 10-19. https://doi.org/10.1016/j.carbpol.2013.12.079

803 Saavedra-Leos, M.Z., Leyva-Porras, C., Araujo-Diaz, S.B., Toxqui-Teran, A., Borras-
804 Enriquez, A., (2015). Technological Application of Maltodextrins According to the Degree of
805 Polymerization. *Molecules*, 20 (12), 67-81. https://doi.org/10.3390/molecules201219746

806 Selomulya, C. & Fang, Y., (2013). Food powder rehydration. In B. Bhandari, N. Bansal,
807 M. Zhang, P. Schuck (Eds.), *Handbook of Foods Powders* (pp. 379-408)

808 Shrestha, A.K., Ua-arak, T., Adhikari, B.P., Howes, T., & Bhandari, B., (2007). Glass
809 transition behavior of spray-dried orange juice powder measured by differential scanning
810 calorimetry (DSC) and thermal mechanical compression test (TMCT). *International Journal*
811 *of Food Properties*, 10, 661-673. https://doi.org/10.1080/10942910601109218

812 Shojaei, S., Farokhi, M., Omidvar, R., Mottaghitalab, F., Haghighipour, N., Shokrgozar,
813 M.A., Ai, J., (2013). Essential Functionality of Endometrial and Adipose Stem Cells in
814 Normal and Mechanically Motivated Conditions. *Journal of Biomaterials and Tissue*
815 *Engineering*, 3 (5), 581-588. https://doi.org/10.1166/jbt.2013.1115

816 Siemons, I., Politiek, R.G.A., Boom, R.M., van der Sman, R.G.M., & Schutyser,
817 M.A.I., **(2020)**. Dextrose equivalence of maltodextrins determines particle morphology
818 development during single sessile droplet drying. *Food Research International*, 131.
819 https://doi.org/10.1016/j.foodres.2020.108988

820 Sobolewska-Zielinska, J., & Fortuna, T., (2010). Retrogradation of starches and
821 maltodextrins of various origins. *Acta Scientiarum Polonorum Technologia Alimentaria*, 9(1),
822 71-81.

823 Takeiti, C.Y., Kieckbusch, T.G., & Collares-Queiroz, F.P., (2010). Morphological and
824 physicochemical characterization of commercial maltodextrins with different degrees of
825 dextrose equivalent. *International Journal of Food Properties*, 13, 411-425.
826 https://doi.org/10.1080/10942910802181024

827 Traini, D., Young, P.M., Rogueda, P., & Price, R., (2006). The Use of AFM and
828 Surface Energy Measurements to Investigate Drug-Canister Material Interactions in a Model
829 Pressurized Metered Dose Inhaler Formulation. *Aerosol Science and Technology*, 40 (4), 227-
830 236. https://doi.org/10.1080/02786820500543316

831 Wang, Y., Truong, T., (2017). Glass transition and Crystallization in Foods. In B.
832 Bhandari & Y.H. Roos (Eds.), *Non-Equilibrium States and Glass Transition in Foods* (pp.
833 153-172)

834 Weiss, C., McLoughlin, P., & Cathcart, H., (2015). Characterisation of dry powder
835 inhaler formulations using atomic force microscopy. *International Journal of Pharmaceutics*,
836 494, 393-407. https://doi.org/10.1016/j.ijpharm.2015.08.051

White, R.P. & Lipson, J.E.G., (2016). Polymer Free Volume and Its Connection to the Glass Transition. Macromolecules, 49 (11), 3987-4007. https://doi.org/10.1021/acs.macromol.6b00215

Wu, X., Li, X., & Mansour, H.M., (2010). Surface analytical techniques in solid-state particle characterization for predicting performance in dry powder inhalers. *KONA Powder and Particle Journal*, 28, 3-19. https://doi.org/10.14356/kona.2010005

Woo, M.W. & Bhandari, B., (2013). Spray drying for food powder production. In B. Bhandari, N. Bansal, M. Zhang, P. Schuck (Eds.), *Handbook of Foods Powders* (pp. 29-56)

Yoshioka, S. & Aso, Y., (2007). Correlations between Molecular Mobility and Chemical Stability During Storage of Amorphous Pharmaceuticals. *Journal of Pharmaceutical Sciences*, 96 (5), 960-981. https://doi.org/10.1002/jps.20926

Young, P.M., Tobyn, M.J., Price, R., Buttrum, M., Dey, F., (2006). The use of colloid probe microscopy to predict aerosolization performance in dry powder inhalers: AFM and in vitro correlation. *Journal of Pharmaceutical Sciences*, 95 (8), 1800-1809. https://doi.org/10.1002/jps.20660

853 **Graphical abstract:**

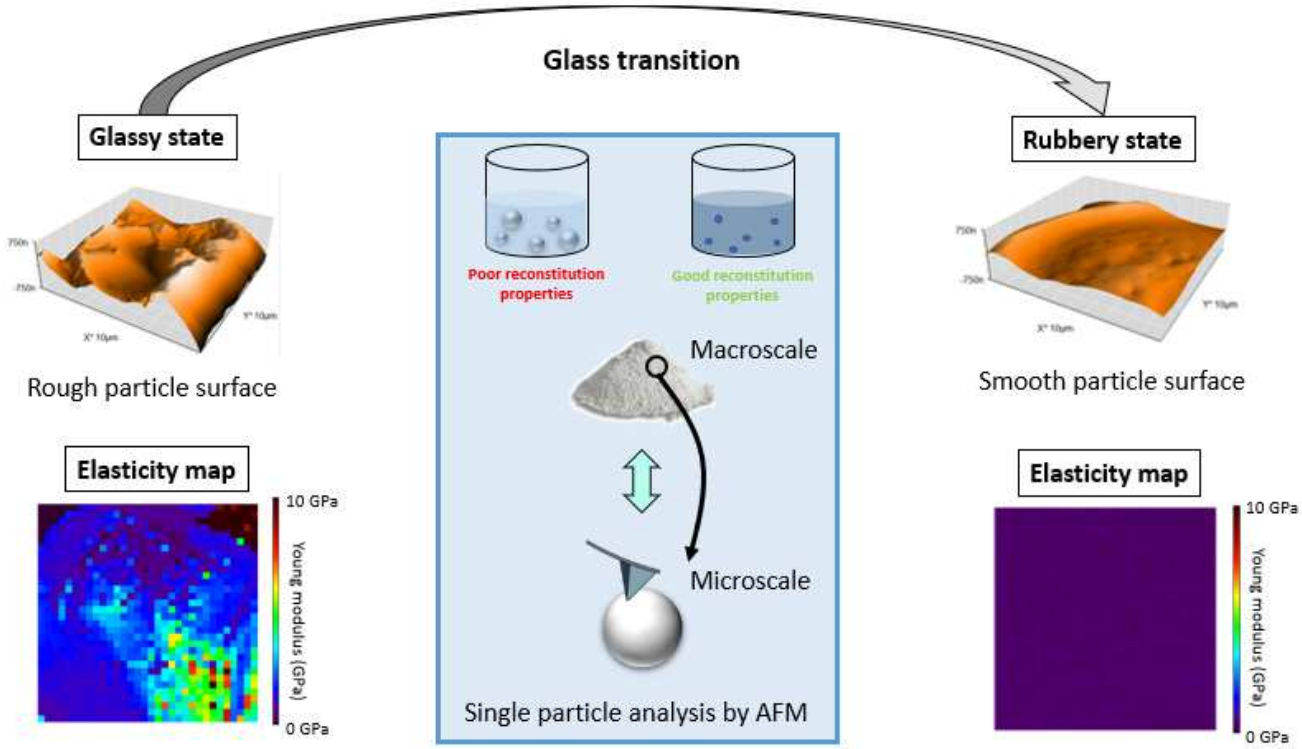

854